ORIGINAL PAPER

Damage Characteristics of Granite Under Hydraulic and Cyclic Loading–Unloading Coupling Condition

Zexu Ning[1] · Yiguo Xue[1] · Zhiqiang Li[1] · Maoxin Su[1] · Fanmeng Kong[1] · Chenghao Bai[1]

Abstract

A series of tests were performed to study the mechanical properties of granite subjected to triaxial cyclic loading–unloading compression under hydro-mechanical coupling. The results show that the damage and permeability evolution of rock are interrelated, and the permeability is closely related to the microfracture propagation during the damage process. The cyclic load magnitude has a controlling effect on the fatigue behavior of the material. When different loading magnitudes are selected, the specimens show different correlation between permeability and residual strain. The correlation analysis between volumetric residual strain and permeability evolution shows that cyclic load not only causes fatigue damage to rock, but also has compaction effect. When confining pressure is larger, the effect of the cyclic load magnitude on the damage will be relatively lower. The linear models of permeability, deformation modulus, radial–axial strain ratio, residual strain, and cyclic load were established to analyze the sensitivity of each parameter to damage. The initial microfractures in granite specimens increase after thermal cycling test, and the P-wave velocity first decreases and then tends to be stable in the whole process. Scanning electron microscope observation shows that more microfractures develop along the axial direction of specimens, which indicates that fatigue damage has directivity.

Highlights

- The larger the confining pressure, the smaller the influence of cyclic load magnitude on the damage.
- High-cycle fatigue behavior shows that rock permeability decreases and the compactness increases.

Keywords Fracture · Damage · Permeability · Hydro-mechanical coupling · Fatigue

1 Introduction

Construction facilities are often subjected to periodic loads (Jafari et al. 2004; Liu and He 2012; Hofmann et al. 2016). The brittle materials such as rocks will exhibit fatigue behavior under cyclic loading, and the compressive strength, plastic deformation and fracture development will change accordingly (Hoshino 1993; Jiang et al. 2006; Liu et al. 2011; Sun et al. 2017; Meng et al. 2020; Ju et al. 2021;

Ning et al. 2021). In different hydro-mechanical coupling environment, the material will also show different mechanical characteristics (Ivars 2006; Li et al. 2014; Wang et al. 2018; Zhang et al. 2019). It is of great significance to study the fatigue behavior of materials subjected to periodic loads for understanding the fatigue life of constructions.

Many researchers have studied the mechanical properties of rock subjected to periodic loads. Xiao et al. (2010) compared six common methods for defining damage variables. Residual strain was considered to be an ideal method due to the description of degradation behavior and consideration on the fatigue initial damage, but it is necessary to consider the selection of data for calculating elastic modulus. Liu et al. (2012) focused on the influence of different confining pressures on the rock fatigue damage characteristics under cyclic loading. The confining pressures had a significant effect on the axial strain of rock specimens during fatigue

---

Zexu Ning and Yiguo Xue Joint first authorship: these authors contributed equally.

✉ Yiguo Xue
xieagle@sdu.edu.cn

[1] Geotechnical and Structural Engineering Research Center, Shandong University, Jinan 250061, China

failure, and the axial residual strain under cyclic loading was described as three phases: initial phase, uniform velocity phase, and accelerated phase. Wang et al. (2013) divided the fatigue behavior of granite subjected to cyclic loading under triaxial compression condition into three stages: the volumetric compaction, volumetric dilation with strain-hardening behavior, and volumetric dilation with strain-softening behavior domains. Through triaxial cyclic loading–unloading test, Meng et al. (2020) found that the post-peak strain-softening characteristics occurred under the low confining pressure ($\sigma_3 \leq 10$ MPa), while the rock specimen demonstrated brittle failure; under the effect of high confining pressure ($\sigma_3 > 10$ MPa), the apparent yield platform (plastic flow deformation) occurred after the peak. Yang et al. (2020) proposed a new loading method for coupled static and dynamic cyclic loading (CSDCL), and the relationships between damage variables and permeability, uniaxial compressive strength, young's modulus were established by fitting.

Fracture initiation and propagation caused by rock damage will also have an impact on permeability (Xue et al. 2015, 2021; Ma and Haimson 2016; Figueiredo et al. 2017; Yang et al. 2017). The permeability in brittle rocks increases due to the propagation of microfractures (Zhang et al. 2013; Shang et al. 2016, 2017; Li et al. 2020). Wang et al. (2012) set up a conceptual model of rock permeability evolution and a micro kinematics mechanism of micro-cracking, forecast the peak permeability evolution of brittle rock. Liu et al. (2016) investigated the permeability evolution of granite gneiss during triaxial creep tests, and found that the permeability remained stable and nearly constant in the steady creep stage and increased rapidly in the accelerated creep stage. Chen (2018) studied the permeability behavior of granite in the process of damage evolution subjected to compressive stress condition, and found that the permeability evolution was closely related to volume strain. Obviously, rock damage and permeability evolution are an interrelated process, but they are rarely studied uniformly. Therefore, it is necessary to study the fatigue damage and permeability evolution of fractured rock mass under hydro-mechanical coupling. Establishing the relationship between rock damage and permeability is helpful to improve the understanding of permeability damage theory of hard rock, and is meaning to know the service life of underground facilities such as water-sealed oil storage caverns.

In this study, a series of tests were performed to study the triaxial cyclic loading–unloading fatigue damage under hydro-mechanical coupling. The fatigue damage characteristics of granite specimens subjected to different confining pressures and cyclic axial stresses were analyzed, and the evolution of permeability, residual strain, deformation modulus and radial–axial strain ratio during the tests was discussed. In addition, P-wave velocity tests and scanning electron microscope (SEM) investigation were performed to reflect the rock damage degree at specific stages. The results could finally serve as references for the stable and low-cost operation of large water-sealed oil storage caverns.

2 Experimental Scheme and Pretreatment

2.1 Equipment

The triaxial cyclic loading–unloading test is performed using Rock Mechanics Test System 815 (MTS-815) (Fig. 1). The
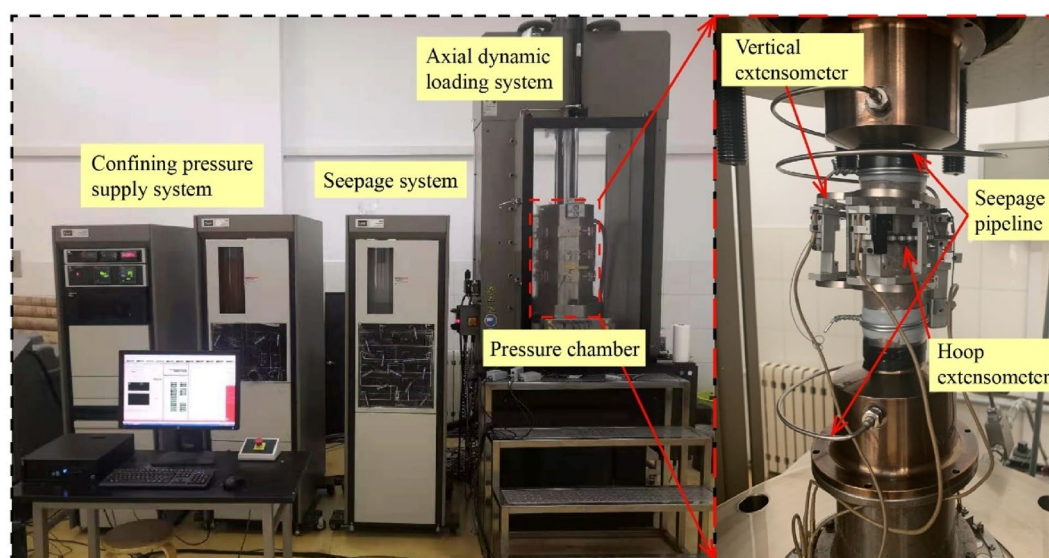

Fig. 1 MTS triaxial cyclic loading–unloading test system

MTS controller consists of hardware components and software applications that provide a closed-loop control of the servo-hydraulic test equipment. This test equipment consists of the following four parts: a compression loading frame, an axial dynamic loading system, a confining pressure supply system and a data acquisition system. The axial dynamic loading system can perform static and dynamic compression tests on rock and concrete specimens under uniaxial and triaxial conditions. It can provide axial pressure up to 4600 kN, pull up to 2300 kN, and lateral confining pressure up to 140 MPa. The load frame assembly includes a fixed crosshead mounted on two rectangular columns bolted to the base plate, creating an extremely rigid yet free-standing frame. Integrated in the base plate is a single-ended, double-acting actuator with a 100 mm (4 in.) stroke for tests requiring large displacements. The frame assembly includes two feedback transducers: a differential pressure transducer and an internal linear variable differential transformer (LVDT) that provides control and measurement of actuator displacement. The triaxial compression test units can simulate dynamic in-situ stress and fluid pressure, and monitor loads, stresses, strains, displacements, fluid pressure, and flow rate in multiple directions using a data acquisition system (6 kHz sampling rate and 16-bit resolution).

2.2 Material Preparation

To serve the project, the in-situ material is selected as the experimental object. The granite specimens used in the tests are the native rock from the underground water-sealed oil storage caverns in the eastern coast of China (Wang et al. 2015; Liu et al. 2018; Li et al. 2019). The main mineral compositions are potassium feldspar, quartz, biotite, and plagioclase. It is observed that the mass ratios of the elements observed is 2.5% C, 45%O, 1.6% Na, 10% Al, 30% Si, 10% K, and less than 1% Cl, respectively. According to the recommendations

of the International Society for Rock Mechanics (ISRM), the rock is processed into cylinders with approximately a height of 100 mm and a diameter of 50 mm (Ulusay and Hudson 2007). After measuring, the average diameter of all granite specimens is 49.6 mm. The physical and mechanical parameters are shown in Table 1, and the integrity is good.

The site selection conditions determine the high integrity and low permeability of the surrounding rock. After observation and measurement, it is found that the selected granites have few natural fractures and extremely low permeability. It is susceptible to measurement error if directly used in permeability test. To strengthen the test effect, reduce the proportion of error and enlarge the rule of test, thermal cycling pre-treatment is performed on granite specimens to increase the number of internal microfractures (Xu and Karakus 2018). As shown in Fig. 2, during the thermal cycling test, the highest heating temperature is set at 300 ℃. After the temperature reaches the default value, the specimens are kept at a constant temperature for 2 h in the heating oven to ensure uniform temperature inside and outside the specimens. After that, the specimens are taken out and quickly put into 10 ℃ water, and the water is quickly changed for 3–4 times. After soaking in water for 2 h, the internal and external temperature of the specimens is stable. After drying the specimens, they are put into the heating oven again to prepare for the next cycle. A total of ten thermal cycles are performed.

To characterize the influence of the thermal cycling test on the specimens, a nonmetallic supersonic instrumentation ZBL-U520 is used to measure the P-wave velocities of saturated specimens. Before each P-wave velocity test, the specimens are saturated with water subjected to negative pressure. Macrofractures appeared on the surface of specimen 1–2. Figure 3 shows the variation of the axial and radial P-wave velocities of some specimens in thermal cycling test. It can be seen that the P-wave velocity of specimens decreases non-linearly

Table 1 Physical and mechanical parameters of granite specimens

Average natural density	Average saturated density	Uniaxial compressive strength	Average elastic modulus	Poisson ratio	Friction angle	Cohesion
2.63 g/cm^3	2.65 g/cm^3	75–104 MPa	29.7 GPa	0.17–0.19	49.2°	10.3 MPa

Fig. 2 Scheme of thermal cycling and P-wave velocity tests
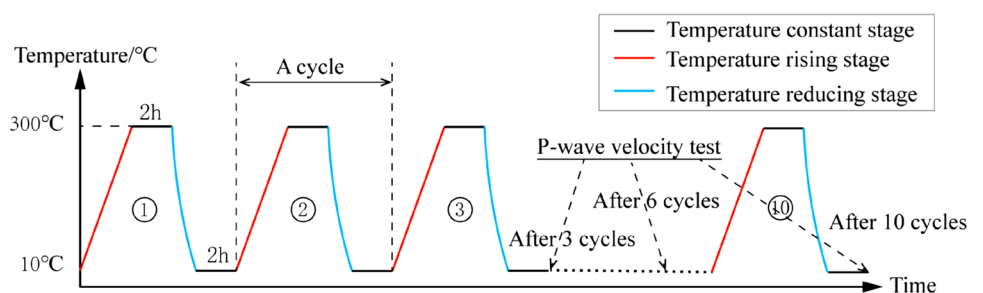
with the increase of cycle number. When the thermal cycles exceed six times, the P-wave velocity tends to be basically stable, indicating that the fracture development is basically stable. The effect of thermal cycling test on the P-wave velocity in the axial direction is more obvious than that in the radial direction, which indicates that the microfracture propagation caused by thermal cycling has a certain directivity. Next, the thermally cycled specimens will be used to perform cyclic loading–unloading test. Damage caused by thermal treatment is not included in damage caused by cyclic loading.

2.3 Experimental Procedure

In this study, triaxial cyclic loading–unloading compression tests are performed. To simulate the real gravity stress in the actual project (about 200 m depth), two different confining pressures are set: 5 MPa and 7.5 MPa. As shown in Fig. 4, after the confining pressure is applied, a hydrostatic pressure of 2 MPa is applied to both sides of the specimen to simulate the hydrostatic environment. The whole test process includes preloading stage, permeability measurement stage and cyclic loading–unloading stage. The cycle loading–unloading stage is non-gradient cycle, 100 times in total. Permeability tests are performed using a transient permeability system after every 10 loading–unloading cycles (Wu and Pruess 2000; Selvadurai et al. 2005), and the hydrostatic pressure at the lower side is increased to obtain a 2 MPa pressure difference. The permeability is calculated by monitoring the dissipation of pressure difference. The transient permeability equation is as follows:

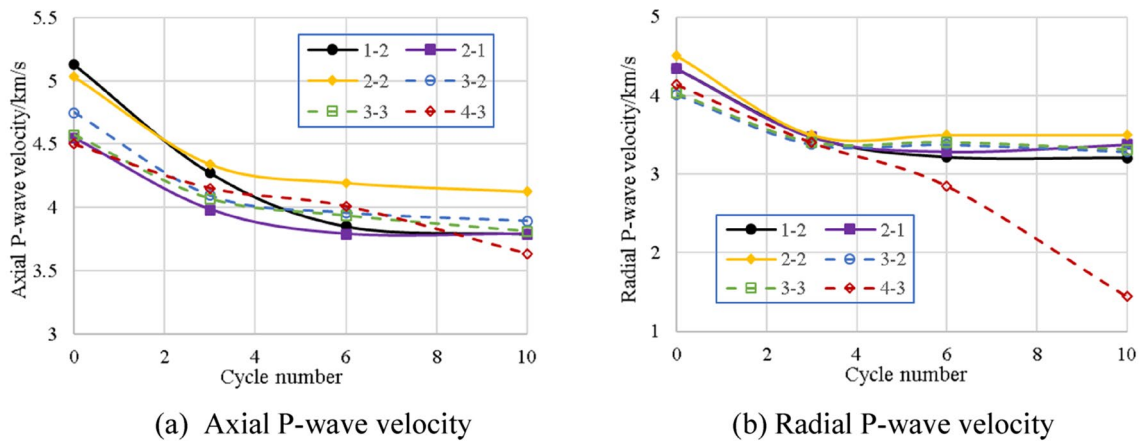$$k = \frac{\mu \beta V L_S \ln\left(\frac{\Delta P_i}{\Delta P_f}\right)}{2 \Delta t A_S}, \tag{1}$$

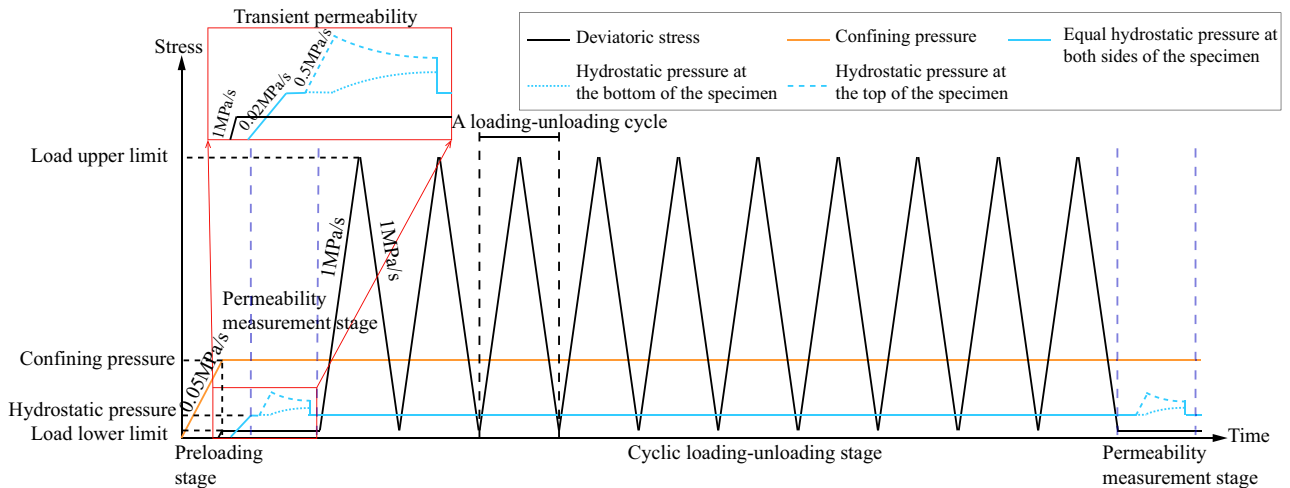Fig. 3 Variation of P-wave velocity in granite specimens during thermal cycling test

Fig. 4 Scheme of triaxial cyclic loading–unloading compression test

where k is permeability, μ is viscosity of fluid, β is compressibility of fluid, V is the reference volume of MTS enhancers, $V = V_1 = V_2 = 175$ cm^3 in this test, ΔP is the pressure differential between the two sides of the specimen through which the liquid passes, $\frac{\Delta P_i}{\Delta P_f}$ is ratio of initial pressure differential to final pressure differential, Δt is the duration of the test, L_S is specimen length, A_S is specimen cross-section area. Figure 5 is a schematic of the transient permeability system, where D_S is specimen diameter. Permeability measurements are also performed before the first cycle and after the last cycle of loading–unloading.

The triaxial compression strength test is performed before the triaxial cyclic loading–unloading test to obtain the triaxial compression strength of granite specimens under different confining pressures (Li et al. 2017). The average triaxial compression strength is 208.4 MPa under 5 MPa confining pressure, and that is 346.9 MPa under 7.5 MPa confining pressure. These are estimated values of the triaxial compression strength of the specimens used in the cyclic loading–unloading test (Kong and Shang 2018). The lower limit of cycle deviatoric stress is set at 10 MPa (offsetting the hydrostatic pressure inside the specimen), and the upper limit is 50%, 65%, and 80% of the estimated values of the triaxial compression strength (Table 2).

3 Experimental Results and Analysis

3.1 Test Under 7.5 MPa Confining Pressure

The load peaks applied in the cyclic loading–unloading are 125 MPa, 160 MPa, and 200 MPa, respectively. Under 7.5 MPa confining pressure, the specimens have been damaged to varying degrees, but no damage has occurred. In
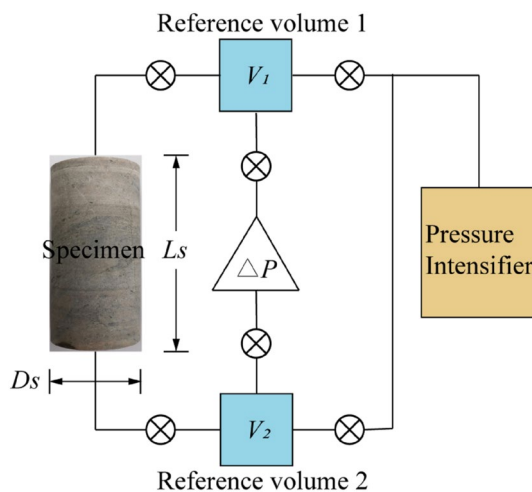
Fig. 5 Simplified schematic of transient permeability system

the whole triaxial cyclic test process, the preloading stage corresponds to the preloading stage of granite specimen, and the cyclic loading–unloading stage corresponds to the cyclic load damage stage.

3.1.1 Stress–Strain Relationship

Figure 6 shows the relationship between the deviatoric stress and the axial strain of the granite specimen under 7.5 MPa confining pressure, in which the axial strain is positive with compression. Because of the heterogeneity, the axial strain of the preloading stage is different. It can be found that during the initial cyclic loading–unloading period, the specimens 1–1 and 2–3 are almost elastic deformation, with little plastic deformation. With the increase of cycle number, the specimens accumulate plastic deformation and produces irreversible axial strain. Judging from the slope of the stress–strain curve, obvious plastic deformation occurred in specimen 3–3 at the initial cycle stage.

Figure 7 shows the relationship between deviatoric stress and radial strain of granite specimen under 7.5 MPa confining pressure, in which the radial strain is positive with stretching. Due to the heterogeneity, the radial strain in the preloading stage is different. Under the action of confining pressure, the radial strain is initially negative, while under the action of cyclic load and confining pressure, the radial strain circulates between positive and negative, and the hysteretic loop is clearly observed. With the increase of cycle number, the position of the hysteretic loop moves, indicating that the specimen produces irreversible radial strain. The moving speed of the hysteretic loop can also reflect the amount of plastic deformation at a stage. The irreversible radial strain occurs with the increase of the cycle number, and the irreversible radial strain accumulation rate gradually increases.

Figure 8 shows the relationship between deviatoric stress and volumetric strain of granite specimens under 7.5 MPa confining pressure, in which the volumetric strain is positive with compression. Due to the heterogeneity, the volume strain of the preloading stage is different, and its magnitude is related to the number and opening of the initial fracture inside specimen. With the increase of the cycle number, irreversible volumetric strain occurrs, and the irreversible volumetric strain accumulation rate gradually decreases.

3.1.2 Relationship Between the Strains

Figure 9 shows the relationship between axial strain and radial strain of granite specimen under 7.5 MPa confining pressure. In the preloading stage, the axial strain and radial strain are negatively correlated, and this proportional coefficient can represent the dominant dip angle of the initial fracture. When the dominant dip angle is closer to 90°, the radial

Table 2 Triaxial cyclic loading–unloading compression of granite specimens

Group	Confining pressure (MPa)	Estimated values of triaxial compression strength (MPa)	Loading–unloading cycle number	Specimen number/load peak (MPa)		
				50%	65%	80%
1	5	208.4	100	5–2/105	1–2/135	3–1/165
2	7.5	246.9	100	1–1/125	3–3/160	2–3/200
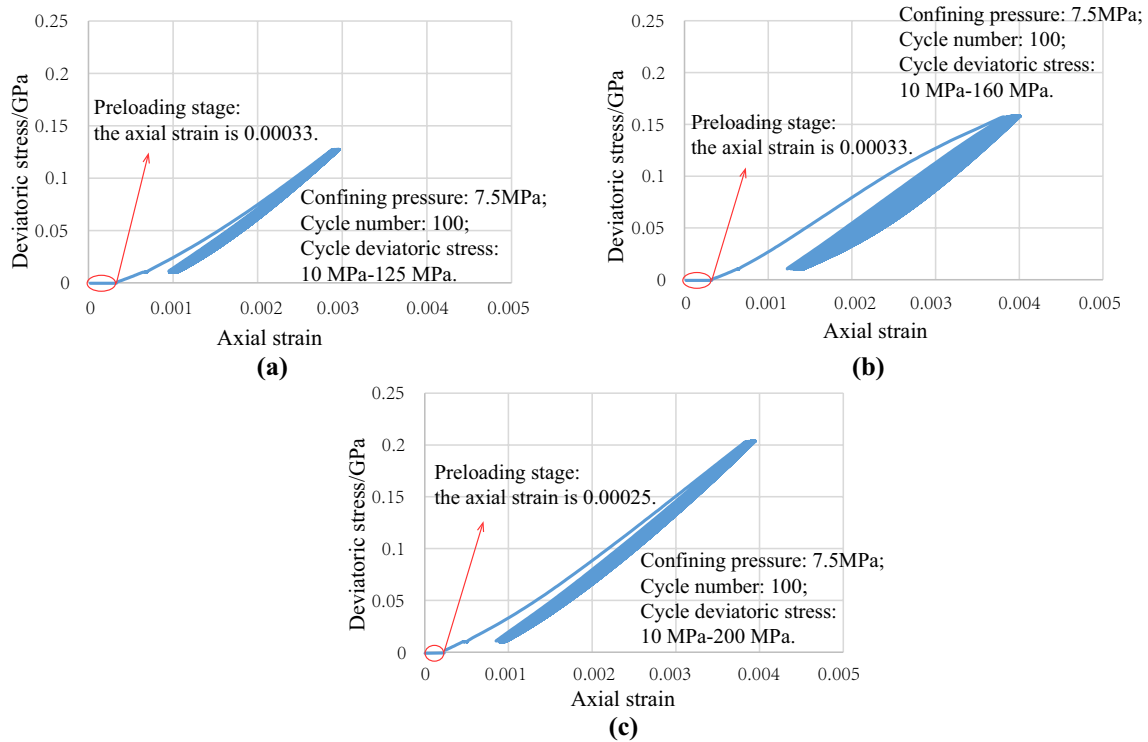
Fig. 6 Relationship between the deviatoric stress and the axial strain under 7.5 MPa confining pressure: **a** 125 MPa load peak, **b** 160 MPa load peak, **c** 200 MPa load peak

strain will be relatively large. If the dominant dip angle is closer to 0°, the axial strain will be relatively large. With the increase of the cycle number, the specimens have obvious irreversible radial strain, which is manifested as the stress hysteresis loop in Fig. 9 moves downward with the increase of the cycle number.

Figure 10 shows the relationship between axial strain and volumetric strain of the granite specimen under 7.5 MPa confining pressure. With the increase of the cycle number, the specimens have obvious irreversible volume strain, which is manifested as the stress hysteresis loop moves upward with the increase of the cycle number.

3.1.3 Damage Characteristics of Cyclic Loading–Unloading

Residual strain is a strain when cyclic deviatoric stress reaches the minimum in the test, including axial residual strain, radial residual strain, and volume residual strain.

When the deviatoric stress is reduced to the minimum in a cycle, the elastic strain part of total strain is reversible, and the remaining irreversible part is the residual strain. When calculating the radial–axial strain ratio and deformation modulus, the calculated value of a loading segment in a loop is selected.

Figures. 11a–c shows the residual strain of the specimen in triaxial cyclic test. When the load peak is 125 MPa and 160 MPa, the axial residual strain of specimen 1–1 and specimen 3–3 increases first and then becomes stable with the increase of cycle number, while the radial residual strain increases first and then decreases. When the load peak is 200 MPa, the axial residual strain of the specimen 2–3 increases first and then decreases, and the radial residual strain increases first and then becomes stable. Due to the low cyclic deviatoric stress, volumetric residual strain of the specimen 1–1 increases first and then becomes basically stable, and the specimen is in volume compression
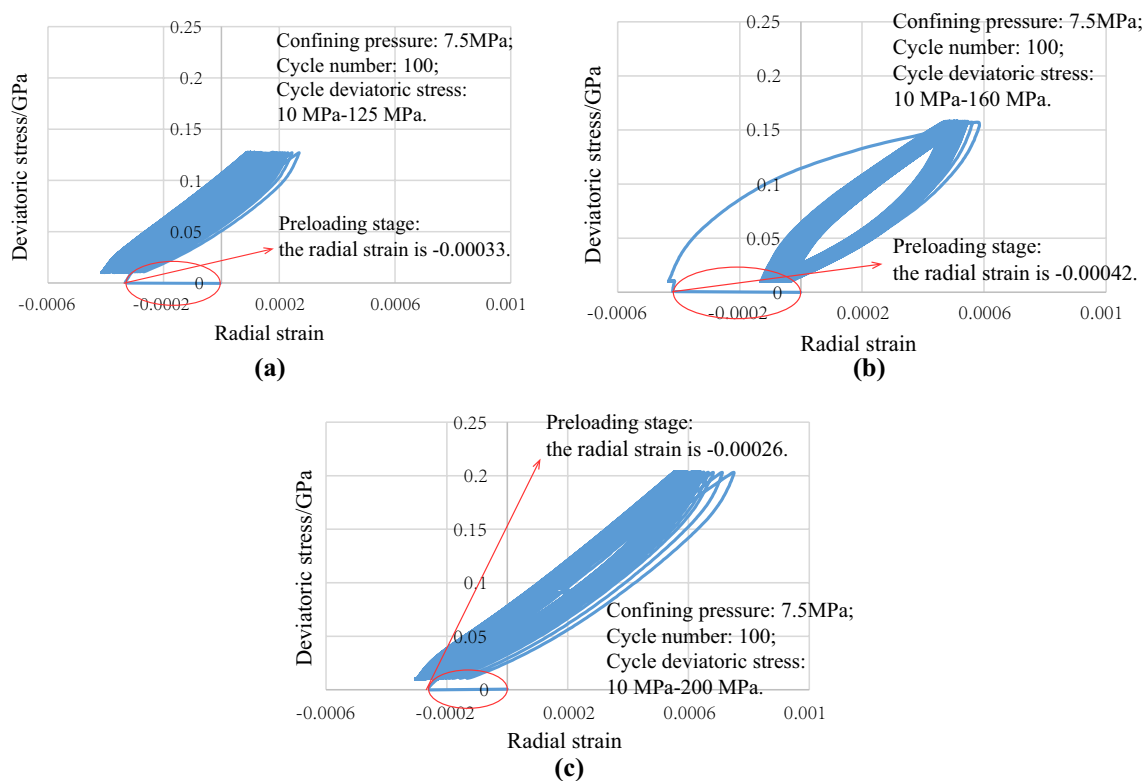
Fig. 7 Relationship between the deviatoric stress and the radial strain under 7.5 MPa confining pressure: **a** 125 MPa load peak, **b** 160 MPa load peak **c** 200 MPa load peak

state. The volume residual strain of specimens 3–3 and 2–3 increases first and then decreases, and the specimens are in volume compression state and volume expansion state. The conclusions are as follows: (1) the cyclic load size and initial integrity are the main factors affecting the fatigue life of granite specimen, (2) when the cyclic stress is large or the specimen has been damaged to a certain extent, with the increase of the cycle number, the axial and radial residual strain will soon pass the cumulative increase stage and begin the decline stage, (3) the small cyclic stress makes the specimen dense and the volume shrinks. When the cyclic stress is large (more than 50% of the triaxial compression strength), the specimen is damaged greatly, becomes loose, and expands after volume compression.

Figure 11d–f shows the fatigue damage of the specimen in triaxial cyclic test: radial–axial strain ratio, deformation modulus, and permeability. It should be noted that influenced by the thermal cycling test and the system error in preloading stage, the first group of data are outliers. When analyzing evolution of radial–axial strain ratio, deformation modulus, and permeability, the first group of data is ignored and analysis is started from the second group. For example, the first group of radial–axial strain ratio data (cycle number is 0) in Fig. 11d are not considered. With the increase of the cycle number, the deformation modulus

of the specimens decreases gradually, and the deformation modulus of the specimen 3–3 is the smallest due to the heterogeneity. The three specimens show different characteristics of radial–axial strain ratio: The strain ratio of specimen 1–1 first decreased to 0, then became negative, increased, and gradually stabilized. The strain ratio of specimen 3–3 changed obviously during the whole test. The strain ratio of specimen 2–3 reached the minimum at about 15 cycles, and then began to increase. When the cycle stress is small, the permeability decreases with the increase of the cycle number. But when the cycle stress is large, the permeability gradually increases. The conclusions are as follows: (1) fatigue damage reduces rock strength, (2) when the damage degree is large, the radial–axial strain ratio will increase, and fatigue failure may happen, (3) when the cyclic load is small, the damage degree is small, the compactness increases, and the permeability reduces. However, when the cyclic load is large, the damage is obvious, the compactness decreases, and the permeability increases. This is consistent with Chen's (2018) research conclusion.

3.1.4 Permeability Evolution During Fatigue Damage

In cyclic loading–unloading test, the physical parameters of specimen evolve when being damaged. Six parameters
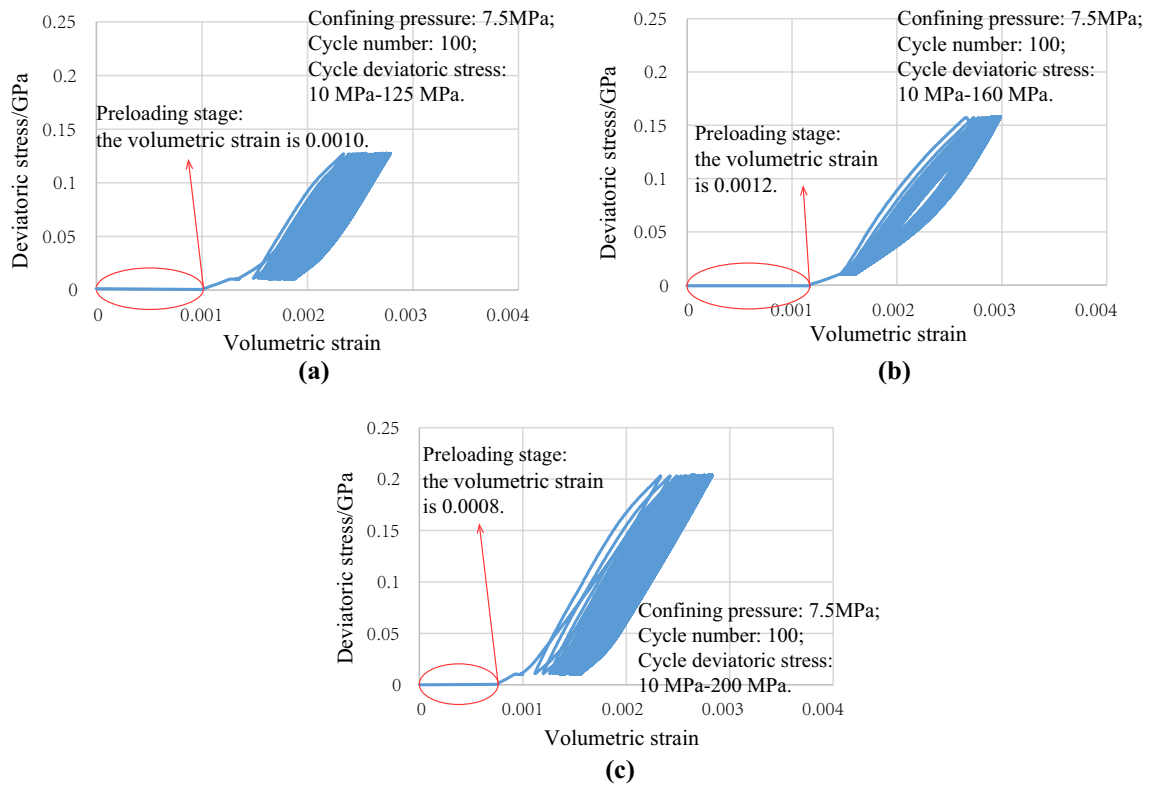
Fig. 8 Relationship between the deviatoric stress and the volumetric strain under 7.5 MPa confining pressure: **a** 125 MPa load peak **b** 160 MPa load peak **c** 200 MPa load peak
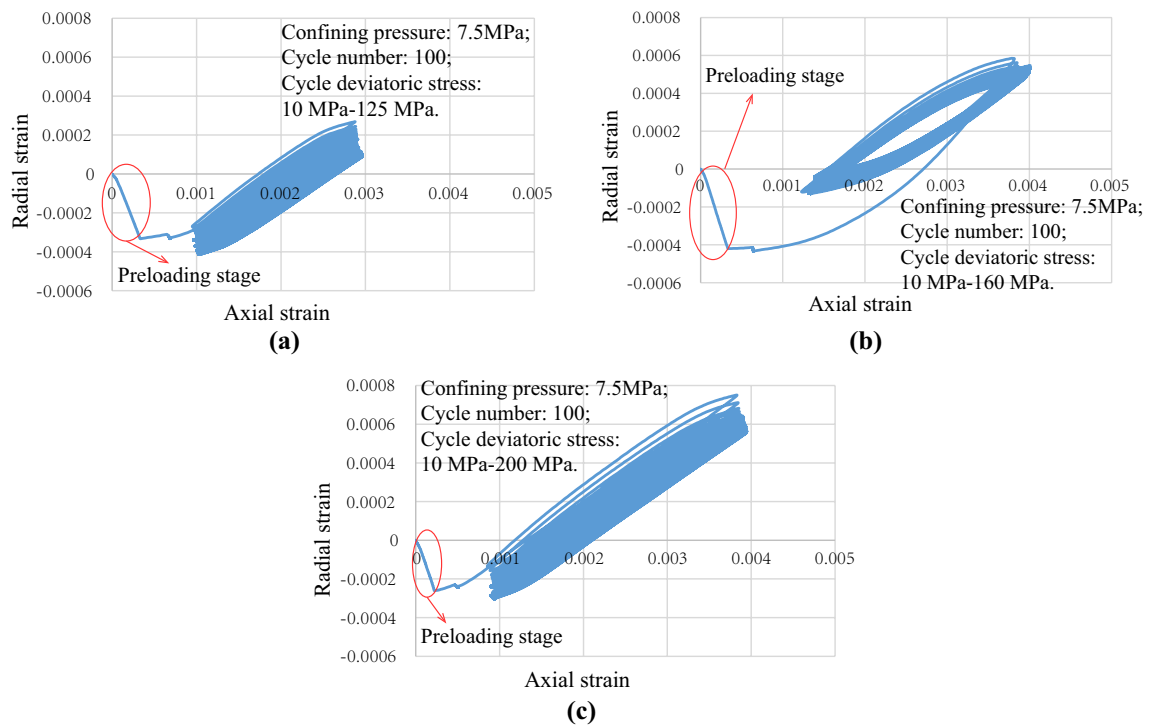

Fig. 9 Relationship between axial strain and radial strain under 7.5 MPa confining pressure: **a** 125 MPa load peak, **b** 160 MPa load peak, **c** 200 MPa load peak
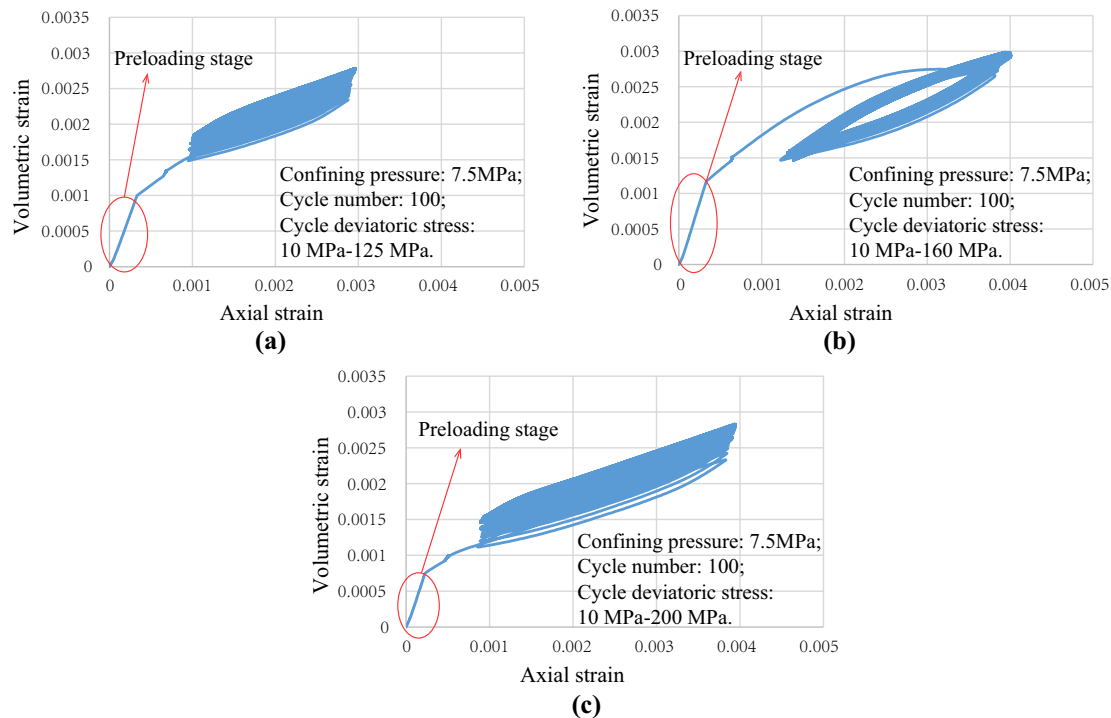
Fig. 10 Relationship between axial strain and volumetric strain under 7.5 MPa confining pressure: **a** 125 MPa load peak, **b** 160 MPa load peak, **c** 200 MPa load peak

are selected: deformation modulus, radial–axial strain ratio, axial residual strain, radial residual strain, volumetric residual strain, and permeability, and these parameters are interrelated. The relationship between permeability and other five parameters is compared emphatically. Figure 12 shows the scatter diagram of the relationships between permeability and other parameters in the test under 7.5 MPa confining pressure. According to the dispersion and trend of scatters in each group, the correlation between permeability and a parameter can be judged.

In contrast, the radial–axial strain ratio has little correlation with permeability. The results show that when the cyclic load is small, the permeability decreases with the decrease of deformation modulus, and decreases with the increase of residual strain. However, when the cyclic load is large (80% of the triaxial compression strength), the permeability decreases with the increase of the axial and volumetric residual strains, while the permeability has no obvious relationship with the deformation modulus and radial residual strains.

3.2 Test Under 5 MPa Confining Pressure

The load peakes applied during cyclic loading–unloading test under 5 MPa confining pressure are 105 MPa, 135 MPa, and 165 MPa respectively. When the load peak is 165 MPa, the failure of specimen 3–1 happens at the 5th cycle. In

addition, according to experimental data, the damage of specimen 1–2 is serious, which is close to fatigue failure.

3.2.1 Damage Characteristics of Cyclic Loading–Unloading

Figure 13 shows the fatigue damage of triaxial cyclic load test under 5 MPa confining pressure. The first group of data in Fig. 13d–f is still ignored in the analysis.

(1) When the load peak is 105 MPa, the residual strain of specimen 5–2 basically stops increasing after about 40 cycles. The total decrease of deformation modulus is not obvious, indicating that the material strength is little damaged. The overall permeability shows a downward trend, indicating that the damage of specimen under this triaxial stress condition is less than the preloading degree, which makes the specimen denser, the fracture closes and the permeability decreases.

(2) When the load peak is 135 MPa, residual strain, the deformation modulus and the radial–axial strain ratio of specimen 1–2 all change obviously. The specimen underwent initial stable damage stage, accelerated damage stage, and pre-peak stable damage stage. The acceleration of residual strain increases first and then decreases, while the reduction rate of deformation modulus increases first and then decreases. The 30–50 cycles are the stage with the most obvious changes in
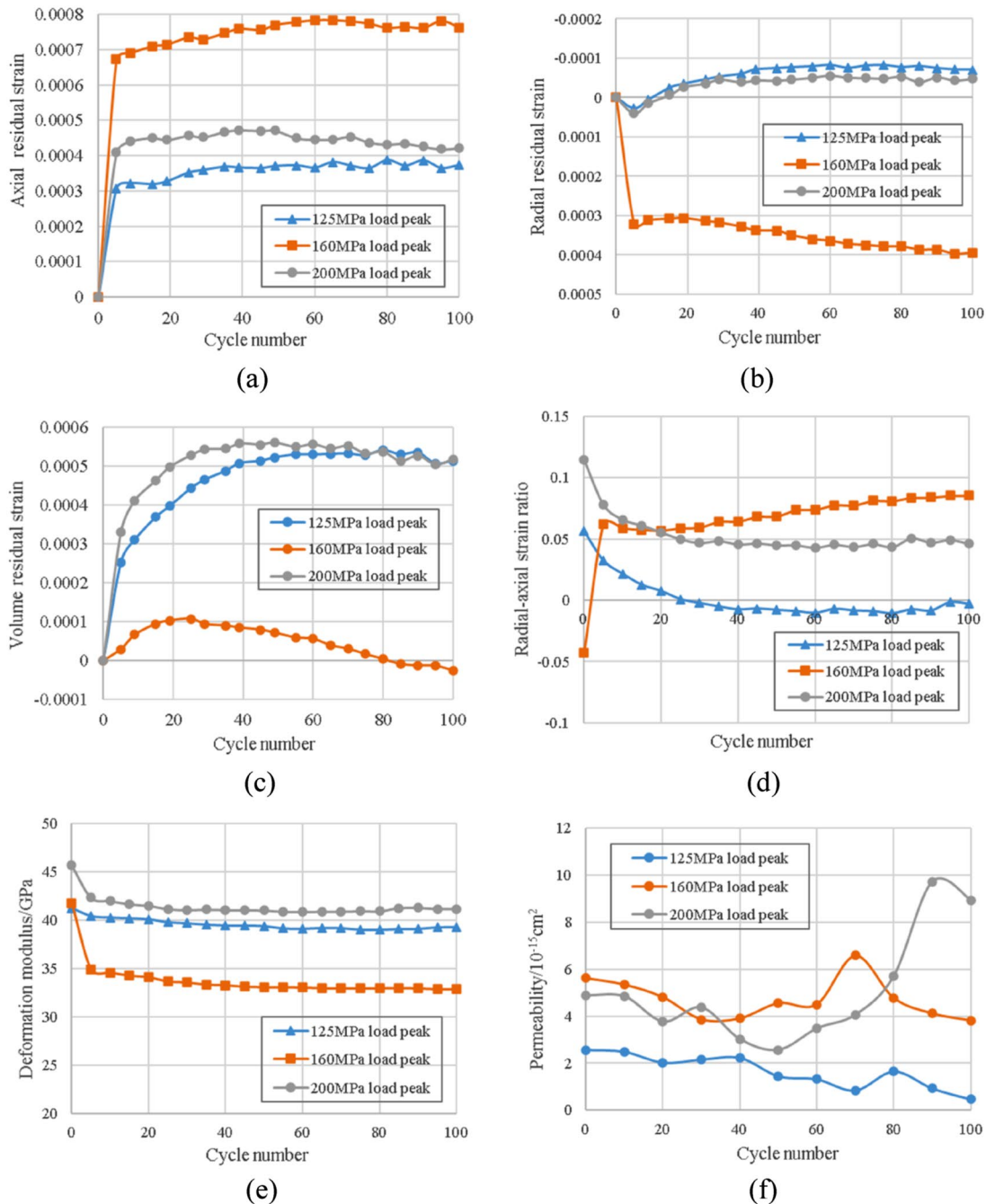
(a)

(b)

(c)

(d)

(e)

(f)

Fig. 11 Fatigue damage of triaxial cyclic load test under 7.5 MPa confining pressure: **a** Relation between axial residual strain and cycle number, **b** Relation between radial residual strain and cycle number, **c** Relation between volumetric residual strain and cycle number, **d** Relation between radial–axial strain ratio and cycle number, **e** Relation between deformation modulus and cycle number, **f** Relation between permeability and cycle number

parameters, and after 50 cycles, it enters the stage of stable accumulated damage. The deformation modulus of the specimen decreases from 44 to 22 GPa. Although the specimen does not happen failure, it can be judged from fracture development degree that the specimen is about to reach the threshold of fatigue failure. The permeability of the specimen increases obviously, and the fastest increase is at 30–50 cycles. It indicates that the strength of the damaged granite decreases obviously, the internal water channels increase.
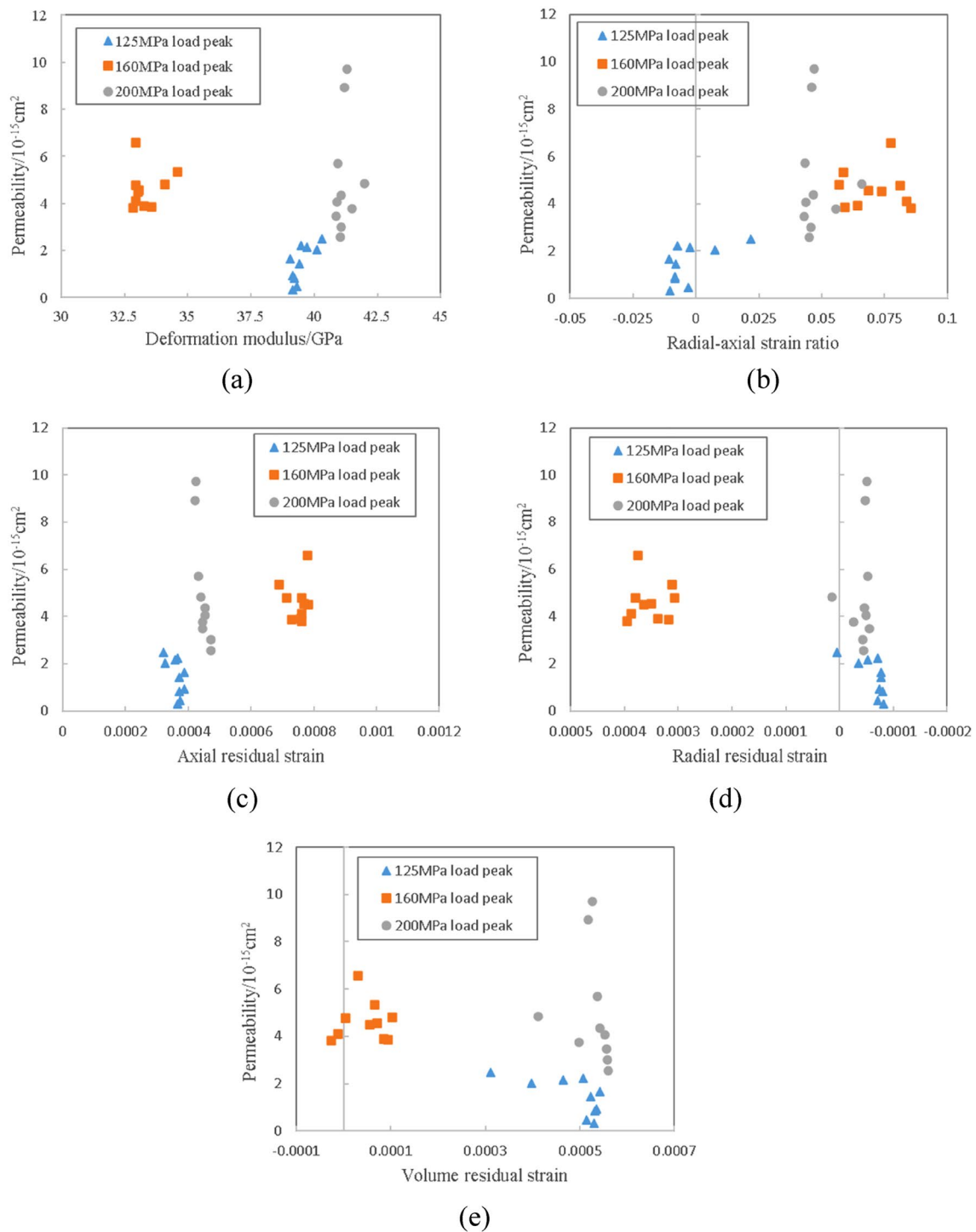
(a)

(b)

(c)

(d)

(e)

Fig. 12 Scatter diagram of the relationships between permeability and other parameters under 7.5 MPa confining pressure: **a** Relation between deformation modulus and permeability, **b** Relation between radial–axial strain ratio and permeability, **c** Relation between axial residual strain and permeability, **d** Relation between radial residual strain and permeability, **e** Relation between volumetric residual strain and permeability

(3) Due to the heterogeneity, when the load peak is 165 MPa, the failure of specimen 3–1 happens at the 5th cycle, and the residual strains increase sharply in the first 4 cycles. After the first loading cycle, the deformation modulus is directly reduced from 44 GPa to less than 25 GPa.
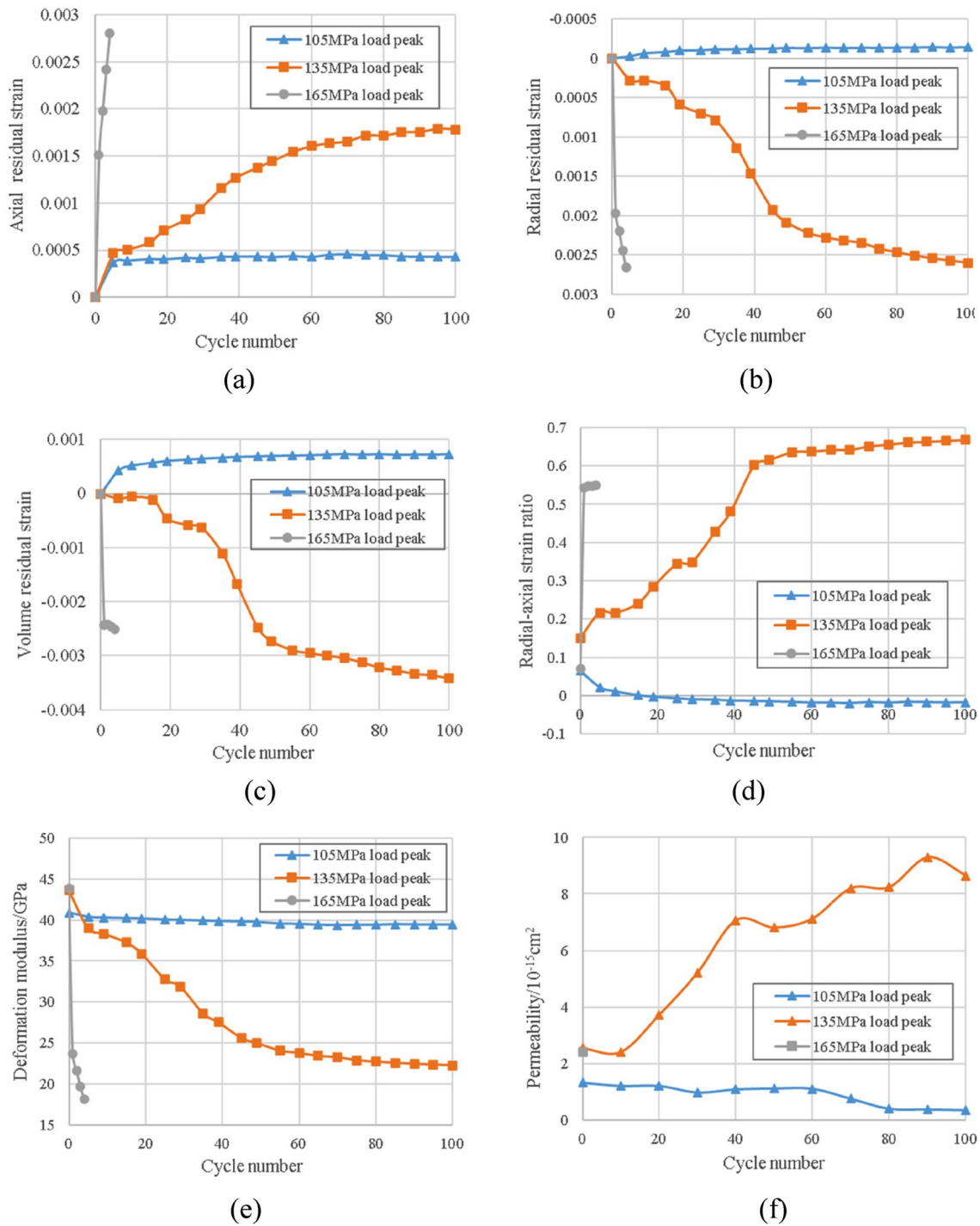
(a)

(b)

(c)

(d)

(e)

(f)

Fig. 13 Fatigue damage of triaxial cyclic load test under 5 MPa confining pressure: **a** Relation between axial residual strain and cycle number, **b** Relation between radial residual strain and cycle number, **c** Relation between volumetric residual strain and cycle number, **d** Relation between radial–axial strain ratio and cycle number, **e** Relation between deformation modulus and cycle number, **f** Relation between permeability and cycle number

3.2.2 Permeability Evolution During Fatigue Damage

Figure 14 shows the scatter diagram of the relationships between permeability and other parameters in the test

under 5 MPa confining pressure. The permeability evolution of specimen 1–2 shows correlation with other parameters, which is due to the obvious damage. According to the results, the permeability is positively correlated with
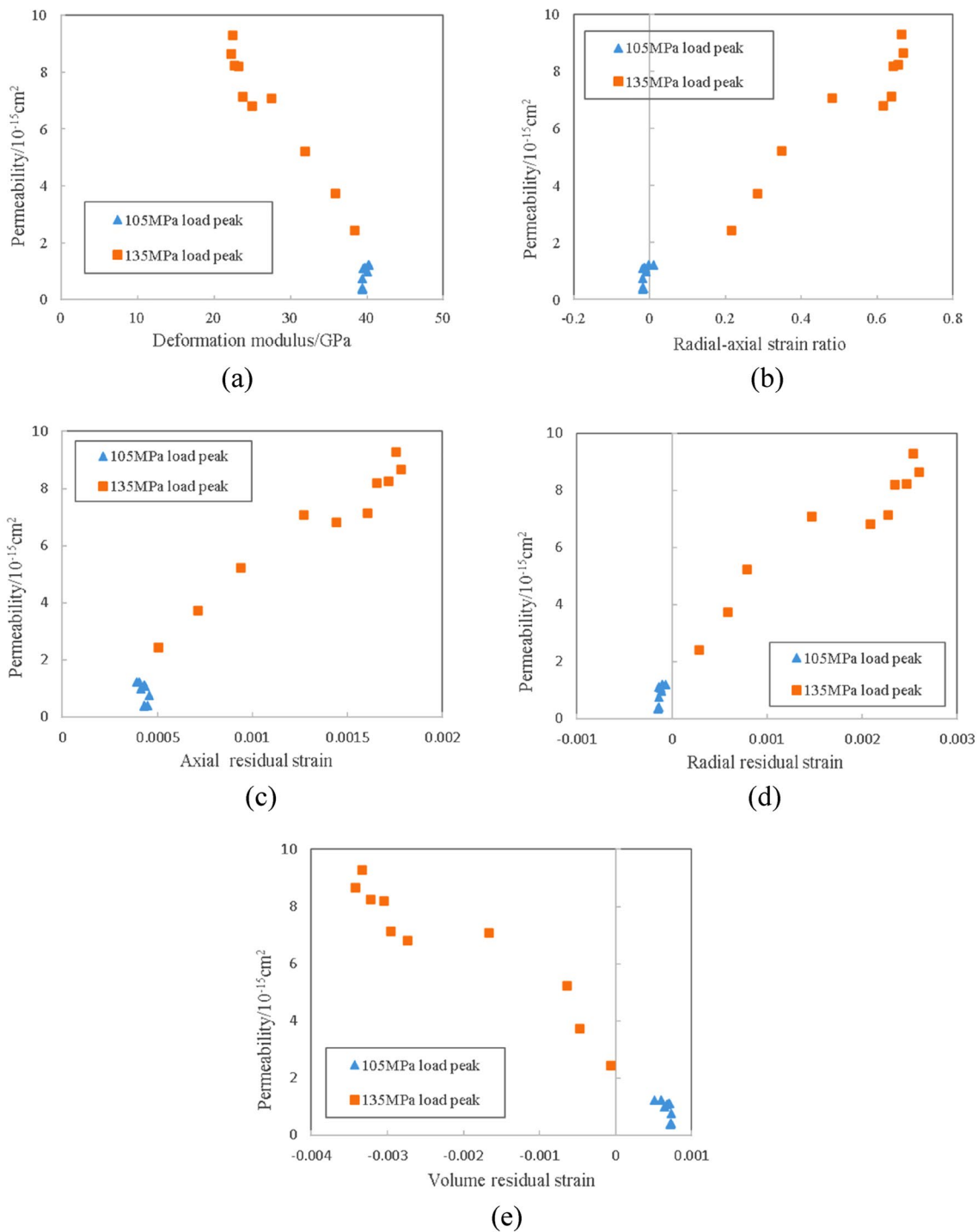
Fig. 14 Scatter diagram of the relationships between permeability and other parameters under 5 MPa confining pressure: **a** Relation between deformation modulus and permeability, **b** Relation between radial–axial strain ratio and permeability, **c** Relation between axial residual strain and permeability, **d** Relation between radial residual strain and permeability, **e** Relation between volumetric residual strain and permeability

the radial–axial strain ratio, axial residual strain, radial residual strain, and volumetric residual strain, and negatively correlated with the deformation modulus. However, the experimental results of specimen 5–2 show the opposite law, and the damage is not obvious. Damage degree has obvious effect on permeability evolution law.
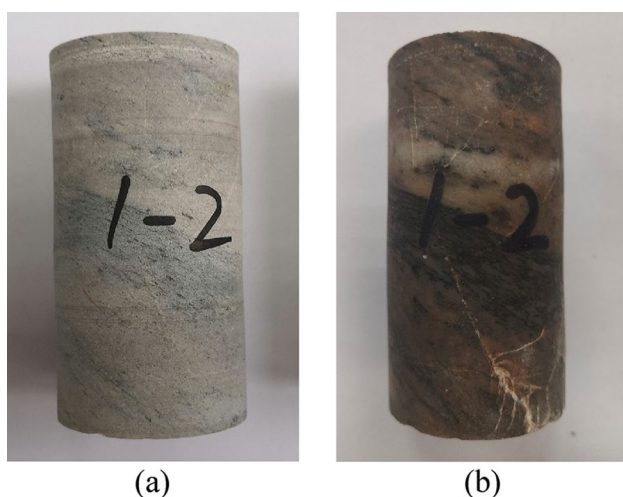
Fig. 15 Fatigue damage of specimen 1–2: **a** before test, **b** after test

3.2.3 Fatigue Damage

Figure 15 shows the specimen 1–2 used in test under 135 MPa load peak and 5 MPa confining pressure. After 100 cyclic loading–unloading, the specimen produce observable macrofractures, but failure does not occurred. The distribution of fractures is not uniform, and microfractures further expand to form macrofractures. It is observed that the fatigue damage behavior of the specimen is obvious, and it can be judged from the change of deformation modulus and residual strain that there are many microfractures in the specimen.

3.2.4 Fatigue Failure

Figure 16 shows the specimen 3–1 used in test under 165 MPa load peak and 5 MPa confining pressure. Fatigue failure occurrs to the specimen in the loading stage after four cycles. It can be seen that the specimen has multiple fracture failure, and the rock fatigue failure is the simultaneous fracture failure of multiple damage fractures.

3.3 Result Analysis After the Test

3.3.1 Fitting Under Different Confining Pressures

Figure 17 compares the relationship between the average of various parameters and load peak. Linear models are fitted for the conditions of 5 MPa and 7.5 MPa confining pressures. Due to the failure of specimen 3–1, the permeability data are not obtained, so the fitting effect is poor. In addition, the fitting effect of the axial and radial residual strains under 7.5 MPa confining pressure is poor, which can be explained

Fig. 16 Fatigue failure of specimen 3–1

by the heterogeneity. According to the results, permeability is not only affected by cyclic load, but also confining pressure conditions. When the confining pressure is small, the cyclic load magnitude has a greater correlation with the radial–axial strain ratio and residual strain, and the effect of cyclic load magnitude on these parameters will be reduced with the increasing confining pressure.

3.3.2 Microstructure Investigated in SEM

The SEM consists of a vacuum system, an electron beam system and an imaging system, which can realize the microscopic observation of rock slices after several times magnification (Xue et al. 2018). The specimens are drilled and cored, and the cores are sliced to obtain circular slices with a 6 mm diameter and a 2 mm thickness, at an angle of 0°, 45°, and 90°, respectively. To compare the damage before and after cyclic loading–unloading test, one side of the cylinder specimen with a height of about 10 mm is cut before the test. The slices taken from this 10 mm cylinder are the slices before the test (Fig. 18a, b). The remaining original cylinder specimen of about 90 mm is cored for the slices after the test (Fig. 18c–f).

The surface microstructure of the slices is observed. Microstructure of the specimen slices under SEM before and after cyclic loading–unloading test is shown in Fig. 18. After comparison, it is found that many microfractures developed inside the specimen after triaxial cyclic loading–unloading tests. The internal microstructure of the specimen is generally broken, and the microfractures are distributed in all directions. The fracture width observed is about 0.3–3 μm, with low penetration and poor water permeability. Such rock masses are still weakly permeable.
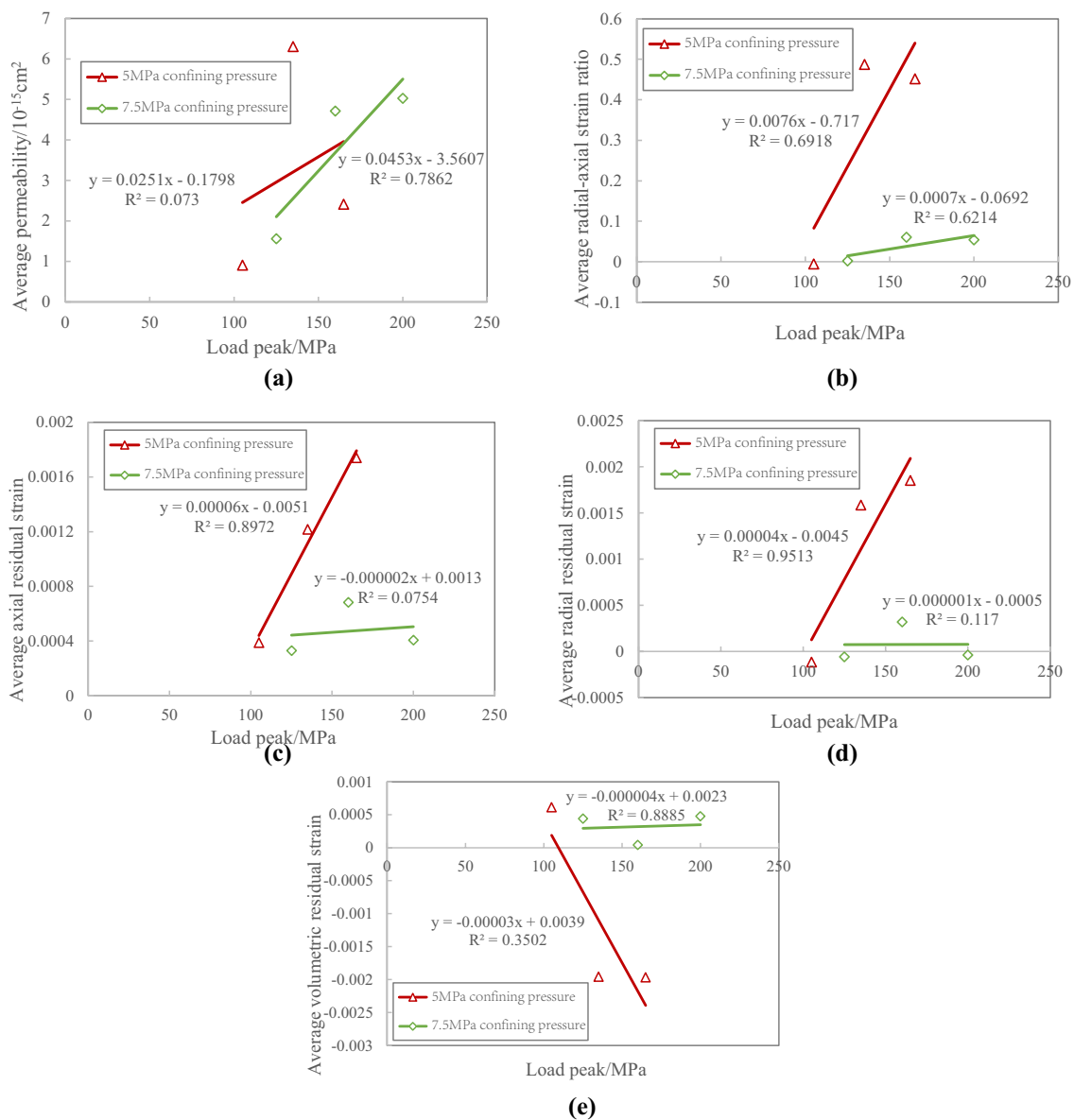
Fig. 17 Fitting relationship between cycle stress and the average of parameters: **a** Relation between load peak and permeability, **b** Relation between load peak and radial–axial strain ratio, **c** Relation between load peak and axial residual strain, **d** Relation between load peak and radial residual strain, **e** Relation between load peak and volumetric residual strain

3.3.3 Comparison of P-Wave Velocities Before and After Triaxial Cycle Test

As shown in the Table 3, the P-wave velocity of the specimens is measured again after the triaxial cyclic test. The results show that the P-wave velocity decreased by 0.3–0.5 km/s after triaxial cyclic test. Damage variables range from 0.15 to 0.30 except for the specimens 1–2 and 3–1. The P-wave velocity of specimen 3–1 are not obtained after failure in the test, and the axial and radial P-wave velocities of specimen 1–2 decrease sharply. The damage variables represented by axial and radial P-wave velocities are 0.897 and 0.993. It indicates that obvious fracture propagation occurred inside the specimen, which is also consistent with the previous test results.

It should be pointed out that the purpose of the cyclic loading–unloading test is to investigate the damage and seepage evolution of saturated granite under different stress conditions, establishing the relationship between damage and permeability. Due to the test cycle number is small, the relationship between cycle number and damage is not discussed. Research on the correlation between fatigue damage and cycle number (fatigue life) will be performed through high-cycle fatigue tests and engineering applications in the future.
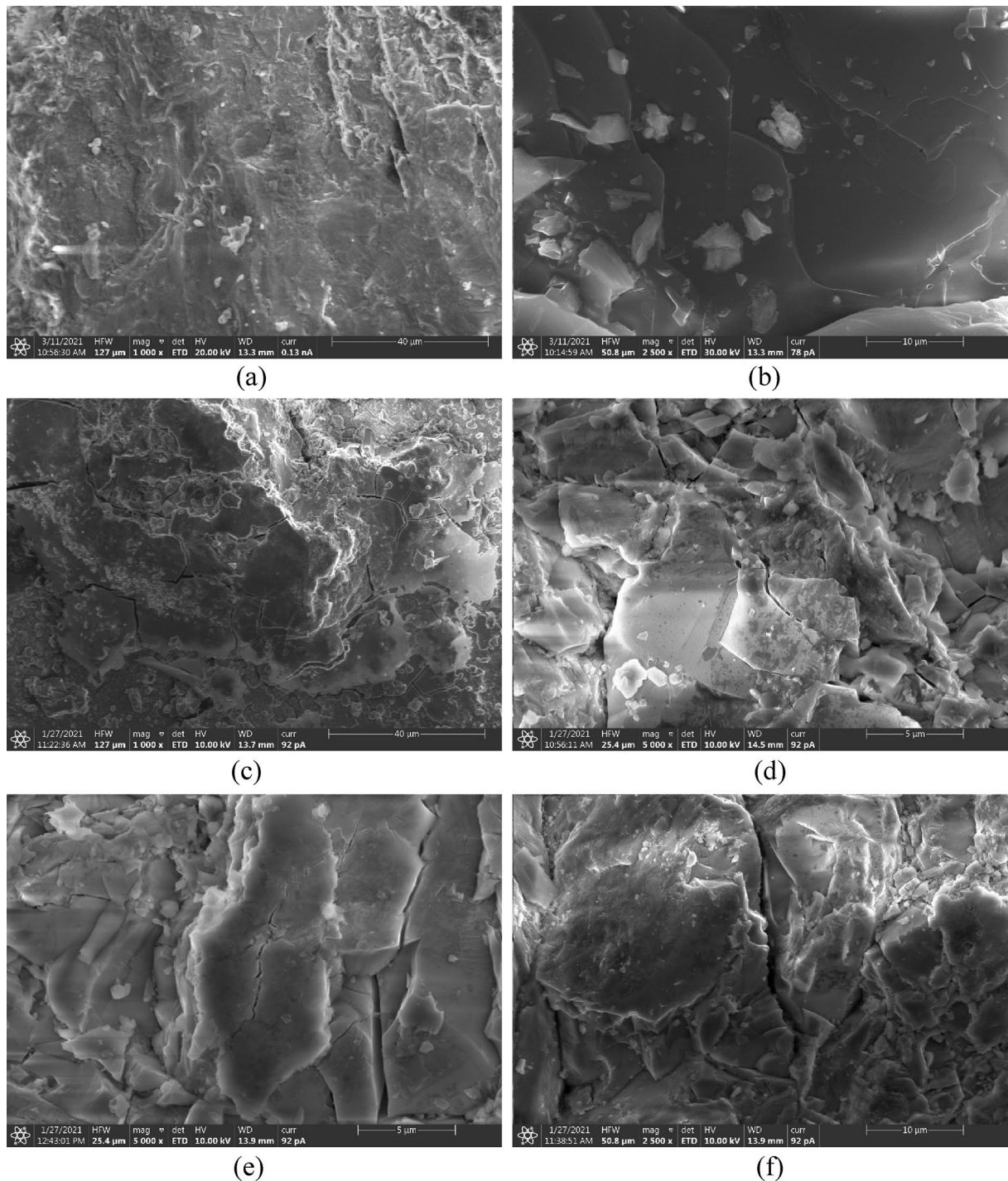
Fig. 18 Microstructure of granite slices before and after cyclic loading–unloading test under SEM: **a** specimen 2–3: 0°–1000 times-before test, **b** specimen 5–2: 90°–2500 times-before test, **c** specimen 2–3: 0°–1000 times-after test, **d** specimen 2–3: 45°–5000 times-after test, **e** specimen 5–2: 0°–5000 times-after test, **f** specimen 5–2: 90°–2500 times-after test

4 Conclusions

In this study, triaxial cyclic loading–unloading tests of granite specimens were performed. The fatigue damage and permeability evolution subjected to different triaxial stress conditions were discussed. The conclusions are as follows:

(1) With the increase of the thermal cycle number, the axial and radial P-wave velocities of the specimens decrease significantly. After 0 cycle, 3 cycles, 6 cycles, and 10 cycles, the average axial P-wave velocities of all granite specimens

Table 3 Comparison of P-wave velocities before and after test

Specimens	P-wave velocities before test		P-wave velocities after test		Damage variable D	
	Axial (km/s)	Radial (km/s)	Axial (km/s)	Radial (km/s)	Axial	Radial
1–1	4.068	3.472	3.405	2.907	0.299	0.299
1–2	3.790	3.205	1.218	0.275	0.897	0.993
2–3	3.934	3.289	3.429	2.717	0.240	0.318
3–1	3.811	3.224	Failure		1	1
3–3	3.810	3.311	3.331	3.049	0.236	0.152
5–2	3.929	3.472	3.532	3.165	0.192	0.169

are 4.642 km/s, 4.088 km/s, 3.965 km/s, and 3.924 km/s, and the average radial P-wave velocities of all granite specimens are 4.180 km/s, 3.409 km/s, 3.307 km/s, and 3.179 km/s. After 4 ~ 5 thermal cycles, the P-wave velocity gradually become stable, indicating that the evolution rate of microfractures inside the specimen also tends to stop.

(2) With the performance of triaxial cyclic loading–unloading tests, different degrees of fatigue deformation and damage occur to granite specimens, which are reflected in the evolution of residual strain, radial–axial strain ratio, deformation modulus, and permeability. The cyclic load magnitude and the content of initial fractures in rock mass are the main controlling factors affecting the fatigue life of specimens. It can be seen from the test results that the cyclic load can not only cause rock damage and expand the specimen volume, but also compaction the specimen to make it denser. The change of permeability depends on the dominant one of this two effects. The larger cyclic load has a greater damage to specimen, and the fracture expansion is greater than the compaction, so the permeability increases, and the deformation modulus usually decreases significantly. On the contrary, the smaller cyclic load increases the compactness of specimen, but decreases the permeability, while the reduction of deformation modulus is not obvious. In the process of cyclic loading–unloading fatigue damage, several parameters of specimen are related to damage, such as deformation modulus, residual strain, and permeability.

(3) SEM observation results show that a large number of microfractures from 0.3 um to 3 um width and different lengths distributed in specimens. On the whole, the microfractures observed in the 90° section are significantly more than those observed in the slices from other angles. That indicates that more microfractures are developed along the axial direction of the specimen. The axial cyclic load has an obvious directional effect on the rock damage.

Declarations

Conflict of interest The authors declare the following financial interests/personal relationships which may be considered as potential competing interests:

References

Chen YL (2018) Permeability evolution in granite under compressive stress condition. Geotech Geol Eng 36(1):641–647

Figueiredo B, Tsang CF, Rutqvist J, Niemi A (2017) The effects of nearby fractures on hydraulically induced fracture propagation and permeability changes. Eng Geol 228:197–213

Hofmann H, Blocher G, Milsch H, Babadagli T, Zimmermann G (2016) Transmissivity of aligned and displaced tensile fractures in granitic rocks during cyclic loading. Int J Rock Mech Min Sci 87:69–84

Hoshino K (1993) Construction of underground caverns for petroleum storage in orogenic areas—geological stability. Eng Geol 35(3–4):199–205

Ivars DM (2006) Water inflow into excavations in fractured rock—a three-dimensional hydro-mechanical numerical study. Int J Rock Mech Min Sci 43(5):705–725

Jafari M, Pellet F, Boulon M, Hosseini K (2004) Experimental study of mechanical behaviour of rock joints under cyclic loading. Rock Mech Rock Eng 37:3–23

Jiang Y, Li B, Tanabashi Y (2006) Estimating the relation between surface roughness and mechanical properties of rock joints. Int J Rock Mech Min Sci 43(6):837–846

Ju MH, Li XF, Li JC (2021) Large-scale asymmetric pulverisation of fault zone: Insights from rock axial strain in static and dynamic loading conditions. Int J Rock Mech Min Sci 137.

Kong F, Shang J (2018) A validation study for the estimation of uniaxial compressive strength based on index tests. Rock Mech Rock Eng 51(7):2289–2297

Li SC, Wang ZC, Ping Y, Zhou Y, Zhang L (2014) Discrete element analysis of hydro-mechanical behavior of a pilot underground crude oil storage facility in granite in China. Tunn Undergr Space Tech 40:75–84

Li XB, Gong FQ, Tao M, Dong LJ, Du K, Ma CD, Zhou ZL, Yin TB (2017) Failure mechanism and coupled static-dynamic loading theory in deep hard rock mining: a review. J Rock Mech Geotech Eng 9(4):767–782

Li ZQ, Xue YG, Li SC, Qiu DH, Su MX, Zhao Y, Zhou BH (2019) An analytical model for surrounding rock classification during underground water-sealed caverns construction: a case study from eastern China. Environ Earth Sci. https://doi.org/10.1007/s12665-019-8606-4

Li Z, Xue Y, Liang J, Qiu D, Su M, Kong F (2020) Performance assessment of the water curtain system: a monitoring system in an underground water-sealed oil reservoir in China. B Eng Geol Environ. https://doi.org/10.1007/s10064-020-01792-0

Liu EL, He SM (2012) Effects of cyclic dynamic loading on the mechanical properties of intact rock samples under confining pressure conditions. Eng Geol 125:81–91

Liu E, He S, Xue X, Xu J (2011) Dynamic properties of intact rock samples subjected to cyclic loading under confining pressure conditions. Rock Mech Rock Eng 44:629–634

Liu L, Xu WY, Wang HL, Wang W, Wang RB (2016) Permeability evolution of granite gneiss during triaxial creep tests. Rock Mech Rock Eng 49(9):3455–3462

Liu J, Zhao XD, Zhang SJ, Xie LK (2018) Analysis of support requirements for underground water-sealed oil storage cavern in China. Tunn Undergr Space Tech 71:36–46

Ma XD, Haimson BC (2016) Failure characteristics of two porous sandstones subjected to true triaxial stresses. J Geophys Res Solid Earth 121(9):6477–6498

Meng QB, Liu JF, Ren L, Pu H, Chen YL (2020) Experimental study on rock strength and deformation characteristics under triaxial cyclic loading and unloading conditions. Rock Mech Rock Eng 54:777–797

Ning Z, Xue Y, Su M, Qiu D, Zhang K, Li Z, Liu Y (2021) Deformation characteristics observed during multi-step excavation of underground oil storage caverns based on field monitoring and numerical simulation. Environ Earth Sci 80:222

Selvadurai APS, Boulon MJ, Nguyen TS (2005) The permeability of an intact granite. Pure Appl Geophys 162(2):373–407

Shang J, Hencher SR, West LJ (2016) Tensile strength of geological discontinuities including incipient bedding, rock joints and mineral veins. Rock Mech Rock Eng 49(11):4213–4225

Shang J, Hencher SR, West LJ, Handley K (2017) Forensic excavation of rock masses: a technique to investigate discontinuity persistence. Rock Mech Rock Eng 50(11):2911–2928

Sun B, Zhu ZD, Shi C, Luo ZH (2017) Dynamic mechanical behavior and fatigue damage evolution of sandstone under cyclic loading. Int J Rock Mech Min Sci 94:82–89

Ulusay R, Hudson JA (2007) The complete ISRM suggested methods for rock characterization, testing and monitoring, Iskitler, Ankara.

Wang HL, Chu WJ, He M (2012) Anisotropic permeability evolution model of rock in the process of deformation and failure. J Hydrodyn 24(1):25–31

Wang ZC, Li SC, Qiao LP, Zhao JG (2013) Fatigue behavior of granite subjected to cyclic loading under triaxial compression condition. Rock Mech Rock Eng 46(6):1603–1615

Wang ZC, Li SC, Qiao LP (2015) Assessment of hydro-mechanical behavior of a granite rock mass for a pilot underground crude oil storage facility in China. Rock Mech Rock Eng 48(6):2459–2472

Wang Z, Glais Y, Qiao L, Huang A, Liu J (2018) Hydro-geochemical analysis of the interplay between the groundwater, host rock and water curtain system for an underground oil storage facility. Tunn Undergr Sp Tech 71:466–477

Wu YS, Pruess K (2000) Integral solutions for transient fluid flow through a porous medium with pressure-dependent permeability. Int J Rock Mech Min Sci 37(1–2):51–61

Xiao JQ, Ding DX, Jiang FL, Xu G (2010) Fatigue damage variable and evolution of rock subjected to cyclic loading. Int J Rock Mech Min Sci 47(3):461–468

Xu XL, Karakus M (2018) A coupled thermo-mechanical damage model for granite. Int J Rock Mech Min Sci 103:195–204

Xue YG, Li SC, Qiu DH, Wang ZC, Li ZQ, Tian H, Su MX, Yang WM, Lin CJ, Zhu JY (2015) A new evaluation method for site selection of large underground water-sealed petroleum storage depots. Sci China Technol Sci 58(6):967–978

Xue DJ, Zhou HW, Zhao YW, Zhang L, Deng LS, Wang XY (2018) Real-time SEM observation of mesoscale failures under thermal-mechanical coupling sequences in granite. Int J Rock Mech Min Sci 112:35–46

Xue Y, Ning Z, Qiu D, Su M, Li Z, Kong F, Li G, Wang P (2021) A study of water curtain parameters of underground oil storage caverns using time series monitoring and numerical simulation. J Zhejiang Univ Sci A 22(3):165–181

Yang T, Liu HY, Tang CA (2017) Scale effect in macroscopic permeability of jointed rock mass using a coupled stress-damage-flow method. Eng Geol 228:121–136

Yang FJ, Hu DW, Zhou H, Lu JJ (2020) Physico-mechanical behaviors of granite under coupled static and dynamic cyclic loadings. Rock Mech Rock Eng 53(5):2157–2173

Zhang B, Shi L, Yu X, Qi SW (2019) Assessing the water-sealed safety of an operating underground crude oil storage adjacent to a new similar cavern—a case study in China. Eng Geol 249:257–272

Zhang Y, Yu S, Zhu W (2013) Study on Seepage Field of Artificial Water Curtains for Underground Petroleum Storage Caverns in Fractured Rock Mass. In Advances In Civil And Industrial Engineering, Pts 1–4. In: L. Tian and H. Hou, eds., Volume 353–356, Applied Mechanics and Materials, pp. 1666